Electrodeposition of Hierarchically Structured Superhydrophobic Ni-PTFE Composite Coating with Remarkable Corrosion Resistance, Chemical and Mechanical Stability

M. Shamsaee Zafarghandi, N. Pirhady Tavandashti*

Department of Materials Engineering, Science and Research Branch, Islamic Azad University, Tehran, Iran

Abstract

One of the main problems of superhydrophobic coatings is the low mechanical and chemical stability, which limits the industrial applications of these coatings. The purpose of this research is to create Ni-PTFE (Polytetrafluoroethylene) composite coatings with hierarchical morphology by electrodeposition method, in order to increase the corrosion resistance, and to improve the mechanical and chemical stability. Ni-PTFE Composite coatings were fabricated by adding different concentrations of PTFE particles (5, 10, 15, 20, 30, and 40 g/L) into the Ni electrodeposition bath. The effect of PTFE concentration on morphology, wettability, and corrosion resistance of the coatings was investigated. The results showed that when an optimum concentration of PTFE (15 g/L) is introduced in the electrodeposition bath, not only the hierarchical morphology of the Ni coating is preserved; but also the maximum contact angle of 158° and the minimum corrosion current density of 0.03 $\mu A/cm^2$ was achieved. The long-term chemical and mechanical stability tests showed that by embedding of PTFE particles with hydrophobic nature, into the hierarchically structured superhydrophobic nickel coatings, higher mechanical and chemical stability is obtaind.

* Corresponding author.
E-mail address: Pirhady@srbiau.ac.ir (N. Pirhady)
nahidpirhady@yahoo.com

Keywords: Superhydrophobic coating; Electrodeposition; Corrosion; Mechanical stability; Nickel; PTFE.

1. Introduction

Solid surface wettability has attracted much attention in basic research and practical applications. Considerable research has been done on superhydrophobic surfaces since 2004, and superhydrophobic coatings have found many industrial applications, such as easy-to-clean and self-cleaning coatings, anti-fog coatings, antifreeze surfaces, isolation of water and oil, antibacterial surfaces, and medicine [1-3]. Various reviews have been published on different aspects of superhydrophobic surfaces [4-6]. Generally, superhydrophobic surfaces are expressed by a steady-state contact angle higher than 150 ° and a slip angle of less than 10°. It is well-known that the wettability of a solid surface is a function of two main factors: surface chemistry and surface roughness [7]. The chemical composition of the surface determines surface energy and has a strong impact on the solid surface wettability. But, generally a surface cannot be superhydrophobic only by changing the surface chemistry [8]. In fact, it is better that the two factors simultaneously exist.

Several methods have been developed to create superhydrophobic surfaces such as structural patterns, electrospinning [9], sol-gel [10], etching [11], electrochemical deposition [12], etc. Compared to other methods, electrodeposition is a simple, economical and versatile method that have been used for fabrication of superhydrophobic surfaces by many researchers. Using electrochemical method and by adjusting the operation parameters, the hierarchical micro-nanostructure can be obtained, which could trap a large number of air, leading to creation of superhydrophobic surfaces [13].

One of the most important problems of the current industry and society is corrosion, which causes a lot of damage. Generally, corrosion cannot be stopped completely, but many

methods have been applied to reduce corrosion [14-18]. One of the important methods for protecting metallic surfaces from corrosion is the use of superhydrophobic coatings. Electrodeposited superhydrophobic coatings with a hierarchical structure have been developed in recent years by many researchers to prevent corrosion; examples include Ni [13-21], Co [22], Cu [23,24], Ni-Co [25], Ni-Cu [26], Ni-P [27], etc. It is believed that the superhydrophobic coatings reduce contact between corrosive species and the metallic substrate, by creating a layer of air between them. Thus, the corrosion protection performance is improved.

One of the factors that has limited the practical use of the superhydrophobic surfaces with hierarchical structure is the lack of long-term mechanical sustainability. Many super-hydrophobic surfaces, when exposed to mechanical damages, lose their hierarchical structure. Hence, their superhydrophobic properties are decreased. Since the coatings are exposed to various environmental damages, strategies for improving long-term mechanical and chemical stability are very important challenges today. Accordingly, in this work for the first time PTFE (Polytetrafluoroethylene) particles are incorporated in the hierarchical micro-nanostructure of electrodeposited nickel coating. Due to the hydrophobic property of PTFE particles, their embedment can enhance the super-hydrophobicity of the nickel coating. Moreover, in case of mechanical damage and loss of the hierarchical structure, the hydrophobic properties of the coating can be still maintained due to presence of hydrophobic PTFE particles. Thus, long term mechanical stability is achieved.

2. Experimental details

2.1. Fabrication of samples

All chemicals used in this work was purchased from Merck and used without further purification. PTFE particles with average particle size of 1 µm (quoted by the manufacturer) was supplied by Sigma-Aldrich. Low carbon steel (ST37) samples were used as substrates in this study. Surface preparation was performed according to the following steps. First, the samples were polished by using 800 up to 2000 grit sand papers. Then, the samples were degreased ultrasonically in acetone for 30 minutes. After that, the samples were immersed in 10 wt.% HCl solution for 20 seconds, rinsed with DI water and immediately placed in an electrodeposition bath. The composition of the electrodeposition bath is indicated in Table 1. Nickel anode was used for electrodeposition. The bath temperature was kept constant at 60 °C and pH=4. The electrodeposition process was performed in two steps. In the first step, electroplating process was carried out at 3 different current densities 20, 40 and 60 mA/cm^2 for 10 min. In the second step, the constant current density of 50 mA/cm^2 was applied for 1 min. To prepare Ni-PTFE composite coatings with hierarchical micro-nanostructure different concentrations of PTFE particles (5, 10, 15, 20, 30 and 40 g/L) were added to the electrodeposition bath. Hexadecyl trimethyl ammonium bromide (CTAB) as cationic surfactant was used for two purposes: first, to disperse PTFE particles; and second, to charge the particles, helping with the deposition of the cationic particles on the cathode substrate. After electrodeposition, all samples were immersed in a solution of 0.1 M myristic acid in ethanol at room temperature for 6 hours.

2.2. Characterization

The microstructure and morphology of the coatings was investigated by field emission scanning electronic microscope (FESEM, TESCAN MIRA3) at a voltage of 15 kV. X-ray energy dispersive spectroscopy (EDS) was also used to determine the chemical composition of the coatings. Surface chemical composition was studied by Fourier transform infrared spectroscopy (FTIR, Frontier PerkinElmer Spectrum). The crystal structure of the samples

was analyzed by X-ray diffraction technique (XRD, Philips X'Pert MPD) using a voltage of 40 kV and a 40 mA current. For collecting data on each sample the scanning angle was from 30^0 to 90^0 , with a step size of 0.02^0 and the time per step was 40 seconds. The wettability of the surfaces was examined by contact angle measurement. To perform this test, Dinolite microscope (AM-413ZT), Hamilton syringe (with volume of 10 μl) and deionized water were used. The thickness of the coatings was measured by a digital coating thickness gauge model Elcometer 456. Corrosion behavior was investigated using potentiodynamic polarization technique and electrochemical impedance spectroscopy (EIS). The corrosion tests were carried out using a potentiostat EG & G Model 273A with platinum auxiliary electrode, and saturated calomel electrode (SCE) as reference electrode. Sodium chloride solution (3.5 wt.%) was used as a corrosive media. Polarization curves in the range -250 to 750 mV were obtained vs open circuit potential at a scanning rate of 1 mV/s. For EIS studies the frequency range was from 100 kHz to 10 mHz using an AC sine wave with the amplitude of 10 mV. Typically 10 frequencies were assessed per decade.

3. Results and discussion

3.1. Wettability and surface morphology

The morphology and properties of the coatings prepared by electrodeposition are a function of operational variables such as applied current density, deposition time and variables related to the coating bath, such as bath composition and pH. Among these variables, the applied current density is of particular importance [13]. Fig. 1(a-c) presents the FESEM images of the micro-nano hierarchically structured nickel coatings deposited at various applied current densities (20, 40 and 60 mA/cm^2). According to the FESEM images, the microstructures consist of several nano-cones formed randomly on micro-cone structures and a hierarchical morphology is obtained. Such hierarchical morphologies are deposited in two steps. At first

step, a layer of microcones array is deposited at current densities of 20, 40 and 60 mA/cm^2 for 600 seconds. Then, the nanocones are deposited on the surfaces of previously formed microcones at current density of 50 mA/cm^2 for 60 seconds. As observed in Fig. 1 the size of microcones generated at the current density of 20 mA/cm^2 is slightly lower than that of the coating produced at the current density of 40 mA/cm^2. It is also observed that by increasing the applied current density up to 60 mA/ cm^2, the growth rate, and consequently the size of the formed microcones is increased. Similar results were achieved by Hang et al [28]. They proposed that the mechanism of the formation of these micro-nanostructures can be described by the tip-discharge theory. When electrodeposition starts, a great amount of Ni nuclei forms simultaneously onto the metallic substrate, and Ni mostly precipitates as nanoparticles. Then, the larger pyramid shaped nanoparticles, serve as the seeds for the growth of nanocones. In the second step, as the original cones were growing bigger, some secondary nuclei are also formed on the surface of the cones. Hence, the micro-nanocone hierarchical structure is developed.

It is also important to note that in the present work ethylenediamine dihydrochloride was used as a crystal modifier in the electrodeposition bath. In a work by Barati Darband et al [29] nickel nanocone structure was fabricated via a single step electrodeposition technique by using proper amount of crystal modifier. It can be explained as follow: While the growth of conventional coatings by electrochemical deposition method occurs in both horizontal and vertical directions; But, the crystal modifier used in the deposition bath encourages the growth of the coating in a vertical direction, delaying the growth in a horizontal direction, which results in the creation of nano-micro cones.

Current density not only affects the surface morphology of the coating, but also influences the surface energy. The wettability of the nickel coatings was studied by contact angle measurement. As depicted in Fig. 2, the static contact angle of the Ni films prepared at the

current densities of 20 and 40 mA/cm^2 was 155° and 157°, respectively. However, the contact angle of the sample deposited at the current density of 60 mA/cm^2 was 131°. It can be due to the bigger microcone structure of this sample. With reference to Fig. 1, it can be seen that the surface of the coatings deposited at the current densities of 20 and 40 mA/cm^2 has a micro-nano hierarchical structure. Based on Cassie's theory [30], when water is dropped on the surface of such coatings, air pockets are trapped underneath water. Therefore, the highly rough, micro-nano hierarchical structure of the coating allow the water to partially sit on the air pockets trapped inside the grooves, reducing contact area between water and surface. However, for the specimen formed at the current density of 60 mA/cm^2 the sharp points are dropped, which probably led to a reduction in the contact angle. According to the FESEM and wettability test results, in the next part of the work the current density 40 mA/cm^2 was chosen for further investigations based on the incorporation of PTFE in the coating.

Incorporation of PTFE particles into the hierarchical micro-nanostructure of electrodeposited nickel coating can improve the superhydrophobic properties of the coating, due to the hydrophobic nature of PTFE particles. Moreover, in case of mechanical damage and loss of hierarchical structure, it is expected that the hydrophobic property of the coating is still maintained, as a result of the presence of hydrophobic PTFE particles. For this reason, PTFE particles with concentrations ranging from 5-40 g/L were introduced into Ni electrodeposition bath. Microstructure and morphology of the coatings deposited with different PTFE concentrations in electrodeposition bath is shown in Fig. 3. The EDS spectra of the corresponding samples are also shown in Fig. 4. It can be seen from Fig. 3 that the PTFE particles are successfully participated in the coating structure. Moreover, the micro-nano hierarchical structure of nickel coatings is well preserved. When the concentration of PTFE particles in the deposition bath was 5 to 15 g/L, a well distribution of PTFE particles in

the coating is observed (Fig. 3 a-c). But, by increasing the PTFE content in the deposition bath up to 40 g/L agglomeration of the particles increased (Fig. 3 d-f).

The results of EDS elemental analysis (Fig. 4) showed that the main components of the coatings were nickel, iron, and fluorine. Detection of iron is caused by the substrate. Presence of fluorine (F) in the coatings is related to PTFE particles. It indicates that PTFE particles are successfully participated in the Ni coatings. Fluorine concentration can be a measure of the concentration of PTFE incorporated into the coating. Fig. 5 shows the changes of Fluorine concentration in the coating (obtained from EDS results), as a function of PTFE concentration in the deposition bath. It is observed that with increasing the concentration of PTFE particles in the deposition bath to a value of 20 g/L, the PTFE content in the coating increases, and then it reaches a constant value. Actually, by increasing the PTFE concentration in the deposition bath, the probability of agglomeration of particles increases. Agglomeration of particles at higher concentrations is an important factor preventing their participation into the coating.

Contact angles of different nanostructured Ni-PTFE composite coatings are shown in Fig. 6. It is observed that by increasing the concentration of PTFE from 5 to 15g/L, the contact angle increases. By further increase of PTFE concentration in electrodeposition bath, the contact angle of the electrodeposited samples decreases. The maximum contact angle of 158° is achieved for the sample deposited at a concentration of 15 g/L PTFE. As stated before, there are two important factors to create superhydrophobic surfaces: low surface energy, and micro-nano roughness. The contact angle changes for coatings created at different concentrations of PTFE particles can be explained as follows. PTFE particles can have two functions. The first function is the reduction of surface energy due to their hydrophobic nature, and the second function is to influence the surface micro-nano roughness [31]. With respect to SEM images (Fig. 3), it can be seen that when the concentration of PTFE is up to

15 g/L, the micro-nano surface roughness of nickel coating is maintained. Therefore, the micro-nano hierarchical structure of nickel coating, together with the reduction of surface energy due to the presence of hydrophobic PTFE particles, results in minor increasing of the superhydrophobicity of the coatings compared to Ni sample. However, for the coatings with concentration of PTFE higher than 15 g/L in deposition bath, the presence of large agglomerated PTFE particles in the composite structure may have reduced the contact angle, considering that the contact angle of pure PTFE is about 108° [32]. Moreover, the micro-nano hierarchical structure is almost eliminated for the coatings with concentration of PTFE higher than 15 g/L, which can reduce the contact angle.

3.2. Crystal structure

The crystal structure of the coatings was investigated using X-ray diffraction (XRD) technique. The XRD spectra of Ni sample and Ni-PTFE composite coating deposited at PTFE concentration of 15 g/L in electrodeposition bath are shown in Fig. 7. The diffraction peaks in 44.5^0 , 52.0^0 , and 76.5^0 are corresponding to nickel (JCPDS No.65-2865), and the peaks in 44.5^0 , 65.0^0 , and 82.5^0 are related to Fe (JCPDS No.65-4899). The presence of iron peaks is originated from the steel substrate. The presence of peaks related to iron and nickel indicates that the surface is not oxidized. However, in the XRD spectrum of the Ni-PTFE composite coating, only nickel diffraction peaks are observed. This can be due to an increase in the coating thickness by incorporation of PTFE particles. The thickness increased from 5.9±0.2 μm for Ni coating, to 8.4±0.3 μm for Ni-PTFE composite coating. These results are in accordance with the results reported by Iacovetta et al [33].

3.3. FTIR

Surface chemical composition of the coatings was investigated by FTIR method. The FTIR spectra of Ni and Ni-PTFE composite coating deposited at PTFE concentration of 15 g/L in

electrodeposition bath are shown in Fig. 8. As mentioned in the experimental section, the samples were treated in myristic acid solution after electrodeposition in order to decrease the surface energy. Almost same absorbing peaks related to myristic acid is observed for both samples. The peaks at 2849 cm^{-1} and 2917 cm^{-1}, are attributed to the methylene ($-CH_2$) and methyl ($-CH_3$) symmetric stretch. The absorbing peaks at 1471, 1573 and 1702 cm^{-1} are related to carboxyl groups (-COO) [22, 34]. This results indicate the successful formation of the myristic acid layer on the surface of the coatings. Some extra peaks are observed for the Ni-PTFE composite sample at 1190 cm^{-1}, and 1151 cm^{-1} which are attributed to asymmetrical and symmetrical CF2 stretching of PTFE. A weaker peak corresponding to the CF2 wagging is also observed at 688 cm^{-1} [35].

3.4. Corrosion resistance

3.4.1. Polarization

Polarization curves of hierarchically structured Ni coating and Ni-PTFE composite coatings deposited at various concentrations of PTFE particles from 5-40 g/L are shown in Fig. 9. The corrosion parameters extracted from polarization curves by Tafel extrapolation method is also shown in Table 2. According to Fig 9 and Table 2, it is observed that with increasing PTFE concentration in the coating from 5 to 15 g/L, the corrosion current density decreased from 3.1 to 0.03 $\mu A/cm^2$, and then with increasing particle concentration up to 40 g/L, the corrosion current density increased up to 3.6 $\mu A/cm^2$. This means that the highest corrosion resistance amongst composite coatings is related to the coating produced at a concentration of 15 g/L PTFE particles. This can be due to the relationship between hydrophobicity and corrosion resistance. In fact, the super-hydrophobic coating supply a barrier between the electrolyte and the substrate, resulting in increased corrosion resistance. This is in agreement with water contact angle test results; where the greatest contact angle amongst different

composite coatings was achieved for Ni-PTFE- 15 g/L sample. Therefore, it is suggested that the more superhydrophobic surfaces can have higher corrosion resistance. By increasing the water contact angle, the surface is less under attack by corrosive ions. Actually, very small part of real area of a superhydrophobic surface is in contact with corrosive solution and hence the corrosion protection performance is improved. These results are in agreement with the findings of other researchers [13, 36, 37]. Furthermore, when comparing the sample with optimum concentration of PTFE (15 g/L) with Ni sample (0 g/L PTFE), the corrosion current densities are 0.03 and 2.28 $\mu A/cm^2$, respectively. This is due to the fact that by creating a composite coating, the corrosion resistance of the coating is improved.

3.4.2. EIS

Electrochemical impedance spectroscopy (EIS) was also used to investigate the corrosion behavior of hierarchically structured Ni coating and Ni-PTFE composite coatings deposited at various concentrations of PTFE particles from 5-40 g/L. Nyquist and bode curves are shown in Fig.10. The equivalent circuit shown in Fig. 11 was used to fit the results. In this equivalent circuit, R_s is the solution resistance. R_c and CPE_c are the coating resistance and the constant phase element of the coating, respectively. R_p is the polarization resistance, and CPE_{dl} is the constant phase element of the electrical double layer. In this study, due to surface roughness, a constant phase element was used instead of a capacitor [38]. The data extracted from the modelling of EIS curves are shown in Table 3. One of the most important information obtained from the Nyquist curves and can be used to verify the corrosion behavior is the charge transfer resistance. Generally, the charge transfer resistance is directly related to the diameter of the Nyquist curves. For the composite coatings, it is observed that with increasing PTFE concentration from 5 to 15 g/L, the polarization resistance increased, and then it decreased by increasing particle concentration up to 40 g/L. From the Bode plots of Fig. 10 it is also observed that the highest values of low frequency impedance is related to

Ni-PTFE-15 g/L coating. The low frequency impedance is directly related to the corrosion resistance. These results are in accordance with the results of polarization studies and shows that the highest corrosion resistance is associated with the coating deposited in the bath containing 15 g/L PTFE particles. Moreover, it could be seen from Table 3 that the double layer capacitance for the sample created at PTFE concentration of 15 g/L has the lowest value among other systems. Thus, the superhydrophobic coating provides a successful corrosion protection for the substrate. Many researchers have reported similar results [13, 21, 25, 26]. This is due to the air pockets stabilized within the grooves of the coating, which remarkably reduces the penetration of aggressive solution to the surface and improves the corrosion resistance [39]. Besides, by comparing the hierarchicallly structured Ni coating and Ni-PTFE-15 g/L sample it is suggested that the incorporation of PTFE particles into the Ni coating can increase the repulsion of water and corrosive solution, improving the corrosion resistance of the coating.

3.5. Durability

One of the most important problems of superhydrophobic coatings limiting their industrial use is their weak chemical and mechanical stability. Recent efforts have been made to improve long-term chemical and mechanical sustainability. One of the most important fundamentals for superhydrophobicity is the surface roughness. The loss of surface roughness by electrolyte diffusion results in the loss of stability. In this case, the coating may enter the chemical reaction with the environment after exposure to the corrosive media. Therefore, a coarse material forms on the coating, and eliminates its initial roughness over time. Hence, the contact angle of water droplets on the surface decreases, and even the coating may find a hydrophilic character [40]. In general, to achieve optimal superhydrophobic coatings, efforts to increase stability are of great importance. One of the main goals of this study was to

increase chemical and mechanical stability. At first, chemical stability and then mechanical stability are investigated.

3.5.1. Chemical stability

The long-term chemical stability was investigated by measuring the water contact angle as a function of immersion time in a solution of 3.5 wt% sodium chloride. The changes of contact angle with immersion time for Ni sample and the composite coating containing PTFE are shown in Fig. 12. It is observed that for both samples the contact angle decreases with increasing immersion time. However, the reduction of contact angle occures with much lower slope for the coating containing PTFE particles. After 96 hours immersion, the contact angle of the PTFE-free sample decreases from 157 to 79 degrees, and the sample is no more hydrophobic. But, the contact angle of the Ni-PTFE composite coating is reduced from 158 to 133 degrees, keeping its hydrophobic behavior with time. The reason for the increase of chemical stability due to the addition of PTFE particles can be described as below: When PTFE particles enter the coating system, the reaction between the corrosive environment and the surface is reduced due to hydrophobic effect of PTFE. Moreover, since the hydrophobic property of PTFE particles is not influenced by immersion time in corrosive media, they can help to improve surface chemical stability.

3.5.2. Mechanical stability

One of the most frequently used tests to evaluate the mechanical stability of superhydrophobic coatings is mechanical abrasion method. In this test, the superhydrophobic sample is placed on a sandpaper, with a certain weight on the sample. Then the sample under pressure is drawn on the sandpaper and after different distances, the contact angle is measured. In this study, 800-grit sandpaper was used, and the applied load on the superhydrophobic samples was 1500 Pascal. The curve of variations of contact angle with

distance traveled is plotted in Fig. 13. Small variations of contact angle indicates a higher mechanical stability. It is found that the contact angle changes are less for Ni-PTFE coating compared to Ni sample, indicating an increase in mechanical stability by incorporation of PTFE into the Ni coating. In a work by Tam et al [39] superhydrophobic Ni-PTFE electrodeposits showed a very good wear stability, due to presence of PTFE particles in the coating.

By embedding of PTFE particles with hydrophobic nature into the hierarchically structured superhydrophobic nickel coating, after surface abrasion, a new hydrophobic surface in exposed to the environment. Therefore, the mechanical stability is maintained. This mechanism is illustrated schematically in Fig. 14. As shown in Fig. 14a after mechanical damage of Ni sample, the surface will no more be superhydrophobic, due to the destruction of its hierarchical structure. But, for a composite coating containg PTFE particles (Fig. 14b), even after mechanical damage and destruction of hierarchical structure, the presence of PTFE particles give the surface a hydrophobic character, improving the mechanical stability of the coating.

Conclusions

In this study, superhydrophobic Ni-PTFE composite coatings with hierarchical morphology was applied on carbon steel substrates using electrodepsoition method and various coating properties were investigated. For this purpose, initialy the effect of the applied current density on the morphology and properties of the electrodeposited Ni coatings was studied. The results showed that the optimum current density to achieve the best wettability and corrosion resistance of nickel coatings with a hierarchical structure was 40 mA/cm^2. Then, different concentrations of PTFE (5, 10, 15, 20, 30, and 40 g/L) was added to the Ni electrodeposition

bath. The results showed that the highest contact angle was achieved when 15 g/L PTFE particles were introduced into the electrodeposition bath. Moreover, the best corrosion protection performance was obtained for the mentioned coating, and the relationship between microstructure, wettability and corrosion resistance was discussed. The mechanical and chemical stability results showed that PTFE particles in the coating contribute to improved stability due to the hydrophobic nature of PTFE.

References

1. Ma, M. and Hill, R.M. "Superhydrophobic surfaces", *Curr. Opin. Colloid Interface Sci*., **11**, pp. 193-202 (2006).
2. Zhang, X., Shi, F., Niu, J., et al. "Superhydrophobic surfaces: from structural control to functional application", *J. Mater. Chem*., **18**, pp. 621-633 (2008).
3. Guo, Z., Liu, W. and Su, B.L. "Superhydrophobic surfaces: from natural to biomimetic to functional", *J. Colloid Interface Sci*., **353**, pp. 335-355 (2011).
4. Darband, G.B., Aliofkhazraei, M., Khorsand, et al. "A Science and engineering of superhydrophobic surfaces: review of corrosion resistance chemical and mechanical stability", *Arabian J. Chem*., **13**, pp. 1763-1802 (2020).
5. Khan, M.Z., Militky, J., Petru, M., et al. "Recent advances in superhydrophobic surfaces for practical applications: A review", *Europ. Polym. J.*, **8**, p.111481 (2022).
6. Li, W., Zhan, Y., Amirfazli, A., et al. "Recent progress in stimulus-responsive superhydrophobic surfaces", *Prog. Org. Coat*., **168**, p.106877 (2022).
7. Sam, E.K., Sam, D.K., Lv, X., et al. "Recent development in the fabrication of self-healing superhydrophobic surfaces", *Chem. Eng. J*., **373**, pp. 531-546 (2019).
8. Sharma, D.K., Baghel, V., Kumar, R., et al. "Recent Developments in Fabrication of Super-Hydrophobic Surfaces: A Review", *Adv. Ind. Prod. Eng.*, pp. 127-140 (2019). https://doi.org/10.1007/978-981-13-6412-9_12
9. Wang, X., Ding, B., Yu, J., et al. "Engineering biomimetic superhydrophobic surfaces of electrospun nanomaterials", *Nano today*, **6**, pp. 510-530 (2011).
10. Manca, M., Cannavale, A., De Marco, L., et al. "Durable superhydrophobic and antireflective surfaces by trimethylsilanized silica nanoparticles based sol− gel processing", *Langmuir*, **25**, pp. 6357-6362 (2009).

11. Ge-Zhang, S., Yang H., Ni, H., et al. “Biomimetic superhydrophobic metal/nonmetal surface manufactured by etching methods: A mini review”, *Front. Bioeng. Biotech.*,**10**, p.958095 (2022).

12. Haghdoost, A. and Pitchumani, R. “Fabricating superhydrophobic surfaces via a two-step electrodeposition technique”, *Langmuir*, **30**, pp. 4183-4191 (2013).

13. Xiang, T., Ding, S., Li, C., et al. “Effect of current density on wettability and corrosion resistance of superhydrophobic nickel coating deposited on low carbon steel”, *Mater. Des*., **114**, pp. 65-72 (2017).

14. Olugbade, T.O., Abioye, T.E., Farayibi, P.K., et al.“Electrochemical properties of MgZnCa-based thin film metallic glasses fabricated by magnetron sputtering deposition coated on a stainless steel substrate”, *Anal. Lett.*, **54** (10), pp. 1588-1602 (2021).

15. Olugbade, T. and Lu, J. “Characterization of the Corrosion of Nanostructured 17-4 PH Stainless Steel by Surface Mechanical Attrition Treatment (SMAT)”, *Anal. Lett.*, **52**(16), pp. 2454 – 2471 (2019).

16. Olugbade, T., Liu, C. and Lu, J. “Enhanced passivation layer by Cr diffusion of 301 Stainless Steel facilitated by SMAT”, *Adv. Eng. Mater*. **21**, p. 1900125 (2019).

17. Olugbade, T. and Lu, J. “Enhanced Corrosion Properties of Nanostructured 316 Stainless Steel in 0.6 M NaCl Solution”, *J. Bio. Tribo. Corros*., **5,** pp. 38 (2019).

18. Olugbade, T. “Electrochemical characterization of the corrosion of mild steel in saline following mechanical deformation”, *Anal. Lett*., **54,** pp. 1055 – 1067 (2021).

19. Chen, Z., Tian, F., Hu, A., et al. “A facile process for preparing superhydrophobic nickel films with stearic acid”, *Surf. Coat. Technol*., **231**, pp. 88-92 (2013).

20. Hashemzadeh, M., Raeissi, K., Ashrafizadeh, F., et al. “Effect of ammonium chloride on microstructure, super-hydrophobicity and corrosion resistance of nickel coatings”, *Surf. Coat. Technol*., **283**, pp. 318-328 (2015).

21. Rahimi, E., Rafsanjani-Abbasi, A., Kiani-Rashid, A., et al. “Morphology modification of electrodeposited superhydrophobic nickel coating for enhanced corrosion performance studied by AFM, SEM-EDS and electrochemical measurements”, *Colloids Surf. A*., **547**, pp. 81-94 (2018).

22. Su, F., Yao, K., Liu, C., et al. “Rapid fabrication of corrosion resistant and superhydrophobic cobalt coating by a one-step electrodeposition”, *J. Electrochem. Soc*., **160**, pp. D593-D599 (2013).

23. She, Z., Li, Q., Wang, Z., et al. “Novel method for controllable fabrication of a superhydrophobic CuO surface on AZ91D magnesium alloy”, *ACS Appl. Mater. Interfaces*, **4**, pp. 4348-4356 (2012).

24. Niu, S., Fang, Y., Qiu, R., et al. “Superhydrophobic film based on Cu-dodecanethiol complex: preparation and corrosion inhibition for Cu”, *Colloids Surf. A*., **550**, pp. 65-73 (2018).

25. Khorsand, S., Raeissi, K., Ashrafizadeh, F., et al. "Corrosion behaviour of super-hydrophobic electrodeposited nickel–cobalt alloy film", *Appl. Surf. Sci*., **364**, pp. 349-357 (2016).

26. Su, F. and Yao, K. "Facile fabrication of superhydrophobic surface with excellent mechanical abrasion and corrosion resistance on copper substrate by a novel method", *ACS Appl. Mater. Interfaces,* **6**, pp. 8762-8770 (2014).

27. Yu, Q., Zeng, Z., Zhao, W., et al. "Patterned Ni–P Alloy Films Prepared by "Reducing–Discharging" Process and the Hydrophobic Property", *ACS Appl. Mater. Interfaces*, **6**, pp. 1053-1060 (2014).

28. Hang, T., Hu, A., Ling, H., et al. "Super-hydrophobic nickel films with micro-nano hierarchical structure prepared by electrodeposition", *Appl. Surf. Sci*. **256**, pp. 2400-2404 (2010).

29. Barati Darband, G., Aliofkhazraei, M. and Sabour Rouhaghdam, A. "Nickel nanocones as efficient and stable catalyst for electrochemical hydrogen evolution reaction", *Int. J. Hydrogen Energy,* **42**, pp. 14560-14565 (2017).

30. Ran, M., Zheng, W. and Wang, H. "Fabrication of superhydrophobic surfaces for corrosion protection: a review", *Mater. Sci. Technol*., **35**, pp. 313-326 (2019).

31. Wang, Y., Wang, W., Zhong, L., et al. "Super-hydrophobic surface on pure magnesium substrate by wet chemical method", *Appl. Surf. Sci*., **256**, pp. 3837-3840 (2010).

32. Zhang, J., Li, J. and Han, Y. "Superhydrophobic PTFE surfaces by extension", *Macromol. Rapid Commun.,* **25**, pp. 1105-1108 (2004).

33. Iacovetta, D., Tam, J. and Erb, U "Synthesis, structure, and properties of superhydrophobic nickel–PTFE nanocomposite coatings made by electrodeposition", *Surf. Coat. Technol*., **279**, pp. 134-141 (2015).

34. Chen, Z., Li, F., Hao, L., et al. "One-step electrodeposition process to fabricate cathodic superhydrophobic surface", *Appl. Surf. Sci*., **258**, pp. 1395-1398 (2011).

35. Piwowarczyk, J., Jędrzejewski, R., Moszyński, D., et al. "XPS and FT IR Studies of Polytetrafluoroethylene Thin Films Obtained by Physical Methods", *Polymers*, **11**, pp. 1629-1641 (2019).

36. Wang, H., Di, D., Zhao, Y., et al. "A multifunctional polymer composite coating assisted with pore-forming agent: Preparation, superhydrophobicity and corrosion resistance", *Prog. Org. Coat*., **132**, pp. 370-378 (2019).

37. Khorsand, S., Raeissi, K. and Ashrafizadeh, F. "Corrosion resistance and long-term durability of super-hydrophobic nickel film prepared by electrodeposition process", *Appl. Surf. Sci.* **305**, pp. 498-505 (2014).

38. Orazem, M.E. and Tribollet, B. "Electrochemical impedance spectroscopy", Wiley-Interscience: Hoboken, NJ (2008).

39. Tam, J., Jiao, Z., Lau, J.C.F., et al. "Wear stability of superhydrophobic nano Ni-PTFE electrodeposits", *Wear*, **374**, pp. 1-4 (2017).

40. Guo, Z., Zhou, F., Hao, J., et al "Stable biomimetic super-hydrophobic engineering materials", *J. Am. Chem. Soc*., **127**, pp. 15670-15671 (2005).

Dr. Nahid Pirhady Tavandashti received her PhD in Nanomaterials from Institute for Nanoscience and Nanotechnology (INST), Sharif University of Technology in 2015. She has worked on self-healing coatings from 2007, when she started her MSc project. Her research interests are stimuli-responsive micro/nanocontainers, smart and functional coatings, and conducting polymers. Since 2016, she is assistant Professor in Department of Materials Engineering, Science and Research Branch (SRBIAU) of Islamic Azad University in Tehran.

Masoud Shamsaee Zafarghandi was MSc student in the field of corrosion engineering in Department of Materials Engineering, Science and Research Branch (SRBIAU) of Islamic Azad University in Tehran. He received his MSc degree in 2019.

Figure Captions

Fig. 1 FESEM images of micro-nano hierarchically structured nickel coatings electrodeposited at current densities of: (a) 20, (b) 40, and (c) 60 mA/cm^2

Fig. 2 Contact angle of different hierarchically structured nickel coatings electrodeposited at current densities of: (a) 20, (b) 40, and (c) 60 mA/cm^2

Fig. 3 FESEM images of Ni-PTFE coatings fabricated at different PTFE concentrations in electrodeposition bath: (a) 5, (b) 10, (c) 15, (d) 20, (e) 30, and (f) 40 g/L

Fig. 4 EDS spectra of Ni-PTFE coatings fabricated at different PTFE concentrations in electrodeposition bath: (a) 5, (b) 10, (c) 15, (d) 20, (e) 30, and (f) 40 g/L

Fig. 5 Variation of Fluorine in the Ni-PTFE coating as a function of PTFE in the deposition bath

Fig. 6 Contact angles of Ni-PTFE composite coatings deposited at different PTFE concentrations in the electrodeposition bath: (a) 5, (b) 10, (c) 15, (d) 20, (e) 30, and (f) 40 g/L

Fig. 7 XRD spectra of: (a) Ni coating, and (b) Ni-PTFE composite coating deposited at PTFE concentration of 15 g/L in electrodeposition bath

Fig. 8 FTIR spectra of (a) Ni coating, and (b) Ni-PTFE composite coating deposited at PTFE concentration of 15 g/L in electrodeposition bath

Fig. 9 Polariation curves of Ni coating and Ni-PTFE composite coatings fabricated in the electrodeposition bath with varying PTFE concentrations

Fig. 10 (a) Bode and (b) Nyquist plots of of Ni coating and Ni-PTFE composite coatings fabricated in the electrodeposition bath with varying PTFE concentrations

Fig. 11 The equivalent circuits used to fit the EIS data

Fig. 12 Variation of water contact angle as a function of immersion time for Ni and Ni-PTFE composite coating

Fig. 13 Variation of water contact angle as a function of abration length for Ni and Ni-PTFE composite coating

Fig. 14 Schematic illustration of the mechanism of mechanical stability improvement for a superhydrophobic coating by embedding of PTFE particles

Table Captions

Table 1. The bath composition used for electrodeposition

Table 2. The corrosion parameters extracted from the polarization curves

Table 3. Corrosion data extracted from the EIS curves

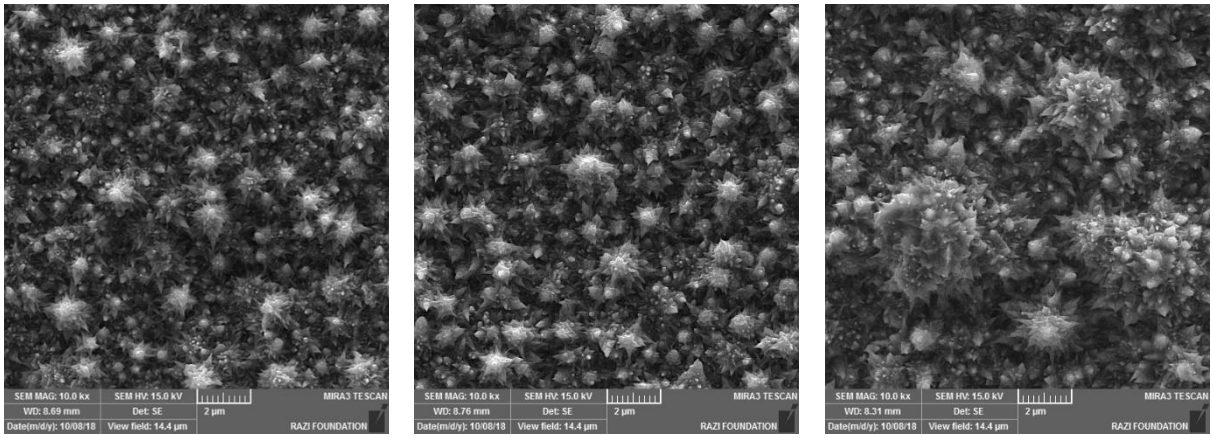
SEM MAG: 10.0 kx
SEM HV: 15.0 kV
WD: 8.69 mm
Det: SE
Date(m/d/y): 10/08/18
View field: 14.4 µm
2 µm
MIRA3 TESCAN
RAZI FOUNDATION
SEM MAG: 10.0 kx
SEM HV: 15.0 kV
WD: 8.76 mm
Det: SE
Date(m/d/y): 10/08/18
View field: 14.4 µm
2 µm
MIRA3 TESCAN
RAZI FOUNDATION
SEM MAG: 10.0 kx
SEM HV: 15.0 kV
WD: 8.31 mm
Det: SE
Date(m/d/y): 10/08/18
View field: 14.4 µm
2 µm
MIRA3 TESCAN
RAZI FOUNDATION

a **b** **c**

Fig. 1

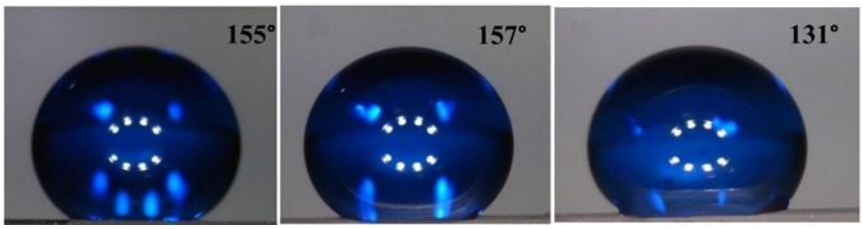
155°
157°
131°

a **b** **c**

Fig. 2

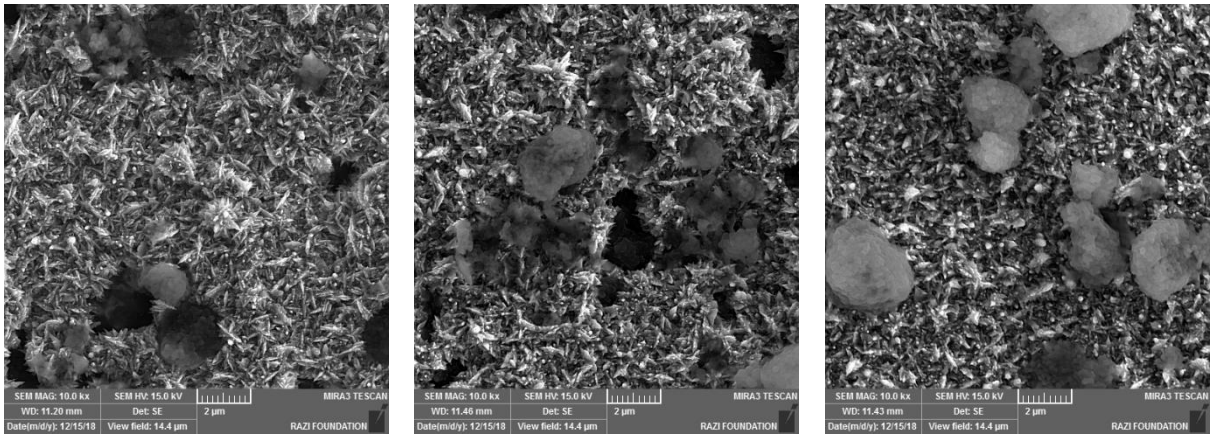
SEM MAG: 10.0 kx
SEM HV: 15.0 kV
MIRA3 TESCAN
WD: 11.20 mm
Det: SE
2 µm
Date(m/d/y): 12/15/18
View field: 14.4 µm
RAZI FOUNDATION
SEM MAG: 10.0 kx
SEM HV: 15.0 kV
MIRA3 TESCAN
WD: 11.46 mm
Det: SE
2 µm
Date(m/d/y): 12/15/18
View field: 14.4 µm
RAZI FOUNDATION
SEM MAG: 10.0 kx
SEM HV: 15.0 kV
MIRA3 TESCAN
WD: 11.43 mm
Det: SE
2 µm
Date(m/d/y): 12/15/18
View field: 14.4 µm
RAZI FOUNDATION

a **b** **c**

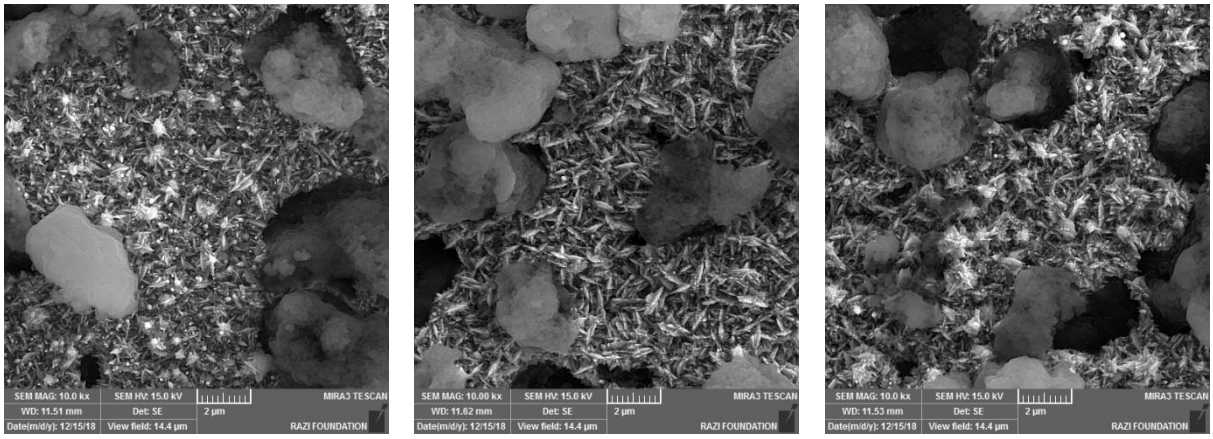
SEM MAG: 10.0 kx
SEM HV: 15.0 kV
WD: 11.51 mm
Det: SE
2 µm
MIRA3 TESCAN
Date(m/d/y): 12/15/18
View field: 14.4 µm
RAZI FOUNDATION
SEM MAG: 10.00 kx
SEM HV: 15.0 kV
WD: 11.62 mm
Det: SE
2 µm
MIRA3 TESCAN
Date(m/d/y): 12/15/18
View field: 14.4 µm
RAZI FOUNDATION
SEM MAG: 10.0 kx
SEM HV: 15.0 kV
WD: 11.53 mm
Det: SE
2 µm
MIRA3 TESCAN
Date(m/d/y): 12/15/18
View field: 14.4 µm
RAZI FOUNDATION

d **e** **f**

Fig. 3

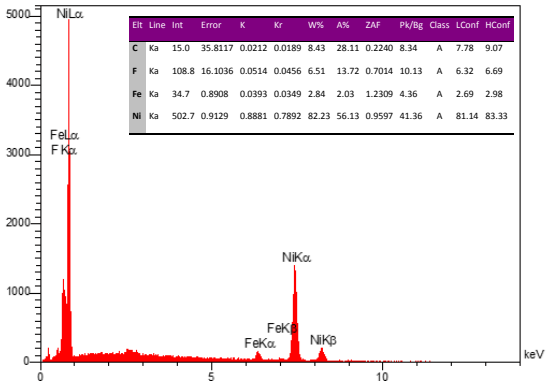
NiLα
FeLα
FKα
NiKα
FeKβ
FeKα
NiKβ
keV
Elt Line Int Error K Kr W% A% ZAF Pk/Bg Class LConf HConf
C Ka 15.0 35.8117 0.0212 0.0189 8.43 28.11 0.2240 8.34 A 7.78 9.07
F Ka 108.8 16.1036 0.0514 0.0456 6.51 13.72 0.7014 10.13 A 6.32 6.69
Fe Ka 34.7 0.8908 0.0393 0.0349 2.84 2.03 1.2309 4.36 A 2.69 2.98
Ni Ka 502.7 0.9129 0.8881 0.7892 82.23 56.13 0.9597 41.36 A 81.14 83.33

a

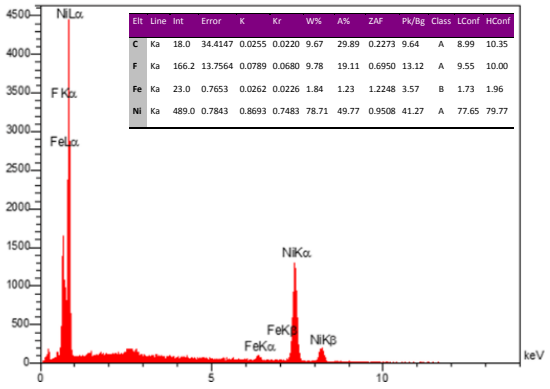
NiLα
FKα
FeLα
NiKα
FeKβ
FeKα
NiKβ
keV
Elt Line Int Error K Kr W% A% ZAF Pk/Bg Class LConf HConf
C Ka 18.0 34.4147 0.0255 0.0220 9.67 29.89 0.2273 9.64 A 8.99 10.35
F Ka 166.2 13.7564 0.0789 0.0680 9.78 19.11 0.6950 13.12 A 9.55 10.00
Fe Ka 23.0 0.7653 0.0262 0.0226 1.84 1.23 1.2248 3.57 B 1.73 1.96
Ni Ka 489.0 0.7843 0.8693 0.7483 78.71 49.77 0.9508 41.27 A 77.65 79.77

b

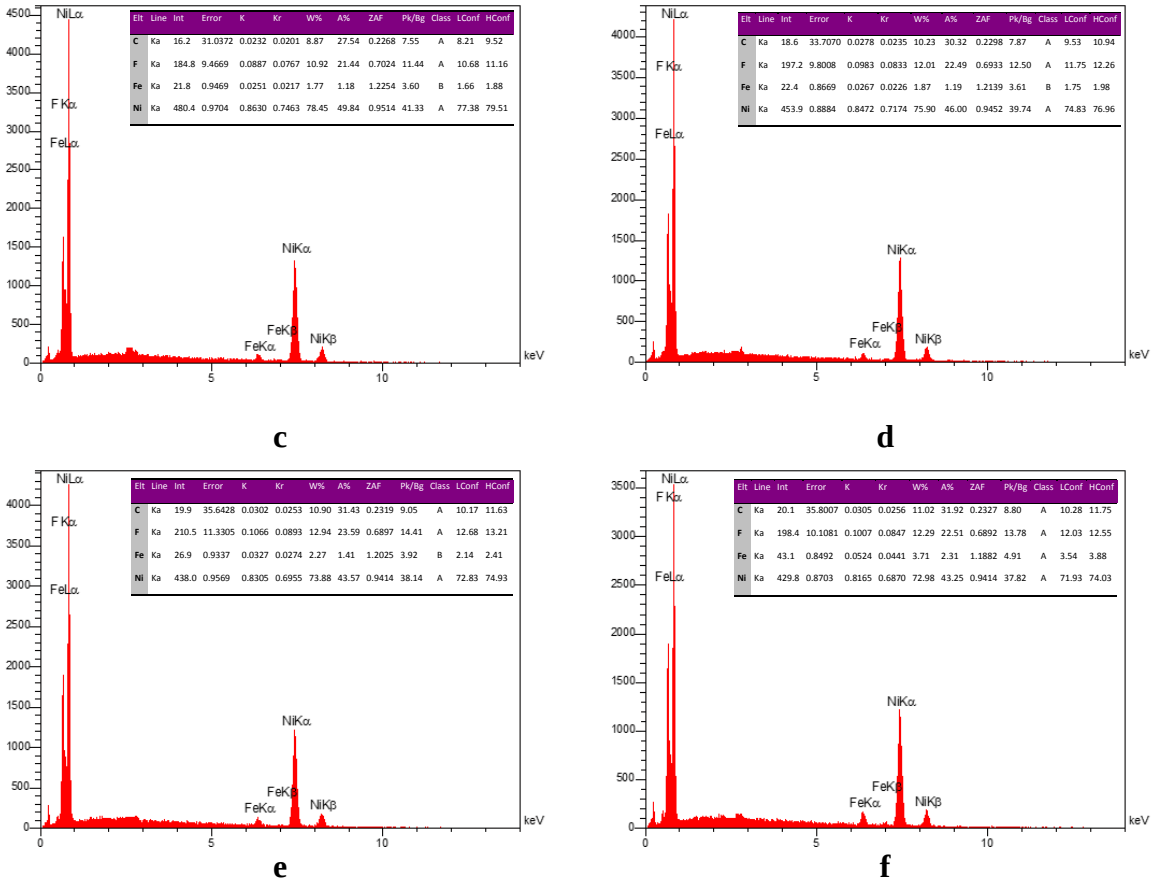
NiLα
FKα
FeLα
NiKα
FeKβ
FeKα
NiKβ
keV
Elt Line Int Error K Kr W% A% ZAF Pk/Bg Class LConf HConf
C Ka 16.2 31.0372 0.0232 0.0201 8.87 27.54 0.2268 7.55 A 8.21 9.52
F Ka 184.8 9.4669 0.0887 0.0767 10.92 21.44 0.7024 11.44 A 10.68 11.16
Fe Ka 21.8 0.9469 0.0251 0.0217 1.77 1.18 1.2254 3.60 B 1.66 1.88
Ni Ka 480.4 0.9704 0.8630 0.7463 78.45 49.84 0.9514 41.33 A 77.38 79.51
c
Elt Line Int Error K Kr W% A% ZAF Pk/Bg Class LConf HConf
C Ka 18.6 33.7070 0.0278 0.0235 10.23 30.32 0.2298 7.87 A 9.53 10.94
F Ka 197.2 9.8008 0.0983 0.0833 12.01 22.49 0.6933 12.50 A 11.75 12.26
Fe Ka 22.4 0.8669 0.0267 0.0226 1.87 1.19 1.2139 3.61 B 1.75 1.98
Ni Ka 453.9 0.8884 0.8472 0.7174 75.90 46.00 0.9452 39.74 A 74.83 76.96
d
Elt Line Int Error K Kr W% A% ZAF Pk/Bg Class LConf HConf
C Ka 19.9 35.6428 0.0302 0.0253 10.90 31.43 0.2319 9.05 A 10.17 11.63
F Ka 210.5 11.3305 0.1066 0.0893 12.94 23.59 0.6897 14.41 A 12.68 13.21
Fe Ka 26.9 0.9337 0.0327 0.0274 2.27 1.41 1.2025 3.92 B 2.14 2.41
Ni Ka 438.0 0.9569 0.8305 0.6955 73.88 43.57 0.9414 38.14 A 72.83 74.93
e
Elt Line Int Error K Kr W% A% ZAF Pk/Bg Class LConf HConf
C Ka 20.1 35.8007 0.0305 0.0256 11.02 31.92 0.2327 8.80 A 10.28 11.75
F Ka 198.4 10.1081 0.1007 0.0847 12.29 22.51 0.6892 13.78 A 12.03 12.55
Fe Ka 43.1 0.8492 0.0524 0.0441 3.71 2.31 1.1882 4.91 A 3.54 3.88
Ni Ka 429.8 0.8703 0.8165 0.6870 72.98 43.25 0.9414 37.82 A 71.93 74.03
f

Fig. 4

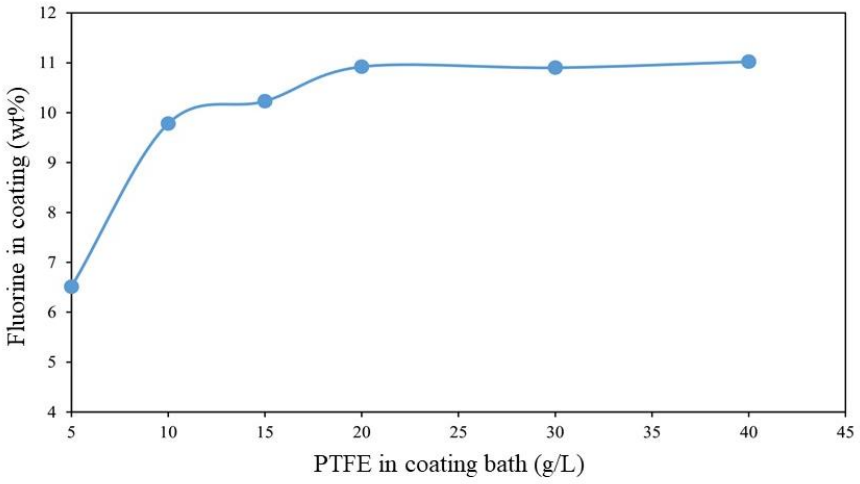
Fluorine in coating (wt%)
PTFE in coating bath (g/L)
12
11
10
9
8
7
6
5
4
5
10
15
20
25
30
35
40
45

Fig. 5

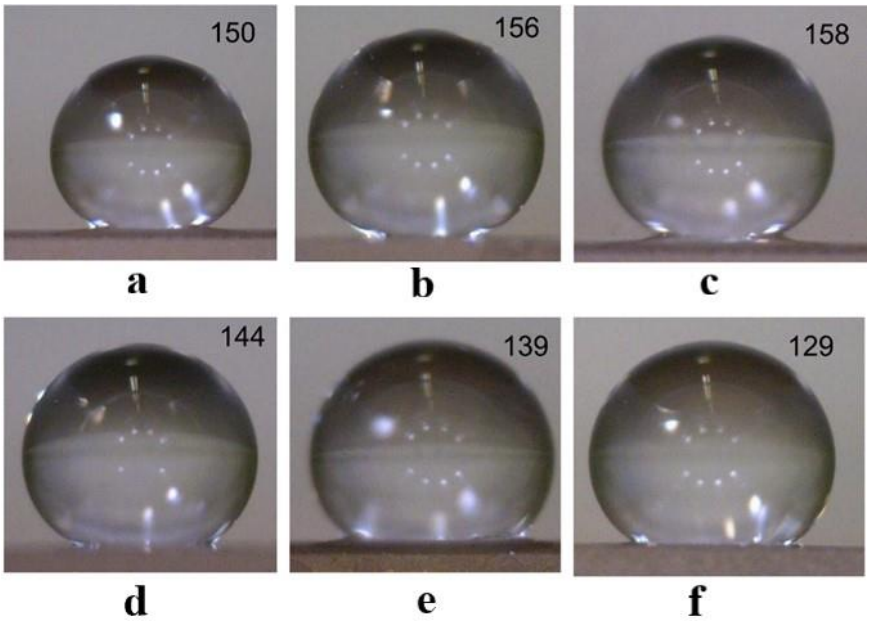

Fig. 6

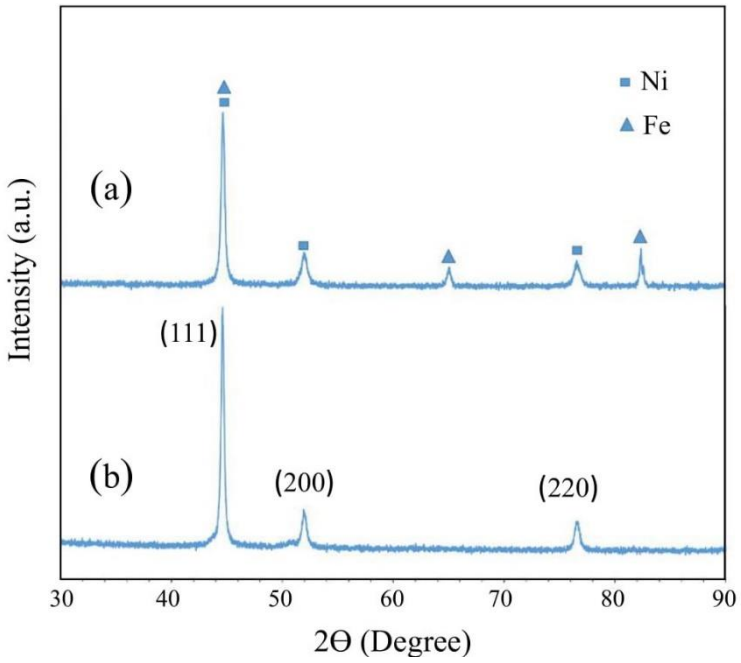

Fig. 7

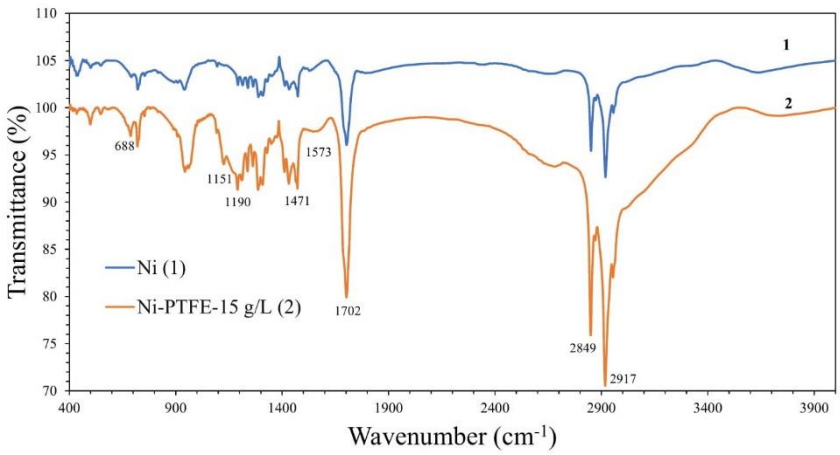
Transmittance (%)
Wavenumber (cm-1)
Ni (1)
Ni-PTFE-15 g/L (2)
1
2
688
1151
1190
1471
1573
1702
2849
2917

Fig. 8

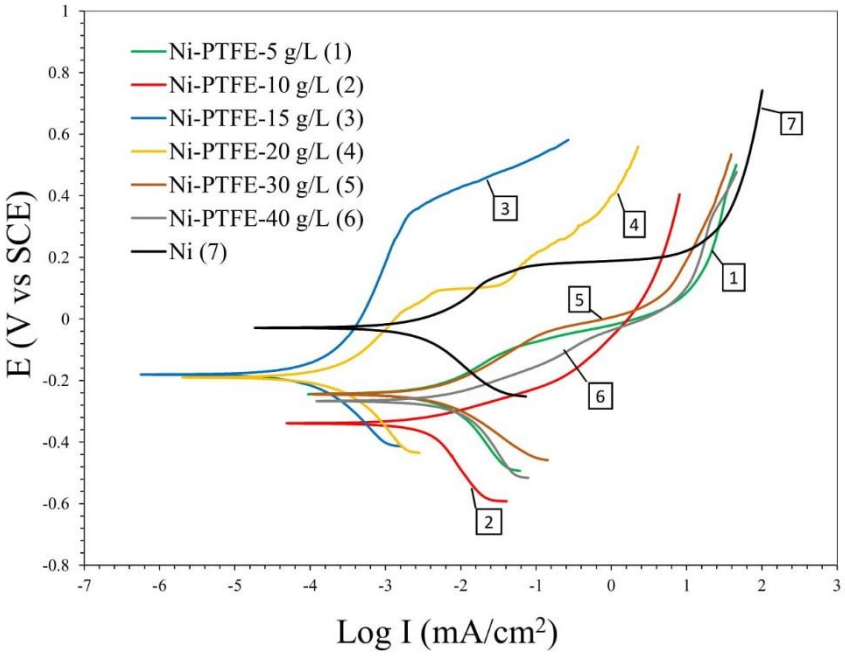
Ni-PTFE-5 g/L (1)
Ni-PTFE-10 g/L (2)
Ni-PTFE-15 g/L (3)
Ni-PTFE-20 g/L (4)
Ni-PTFE-30 g/L (5)
Ni-PTFE-40 g/L (6)
Ni (7)
E (V vs SCE)
Log I (mA/cm2)
1
2
3
4
5
6
7

Fig. 9

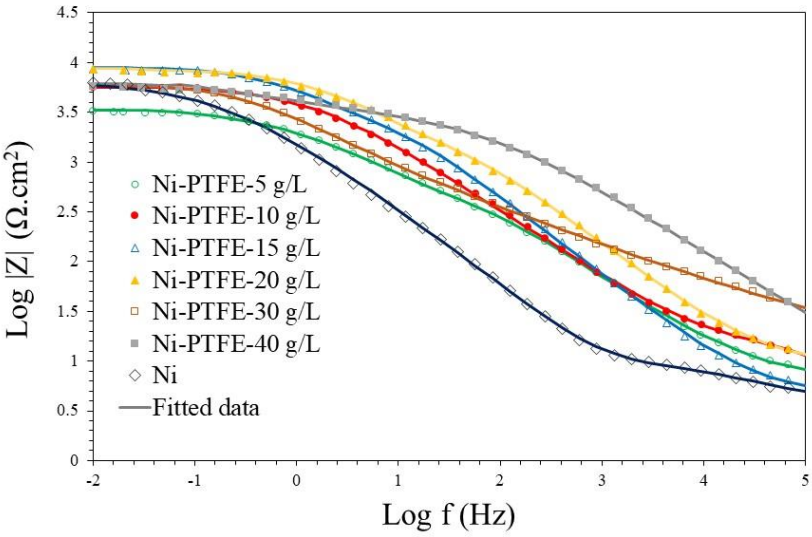
Log |Z| (Ω.cm²)
Log f (Hz)
Ni-PTFE-5 g/L
Ni-PTFE-10 g/L
Ni-PTFE-15 g/L
Ni-PTFE-20 g/L
Ni-PTFE-30 g/L
Ni-PTFE-40 g/L
Ni
Fitted data

a

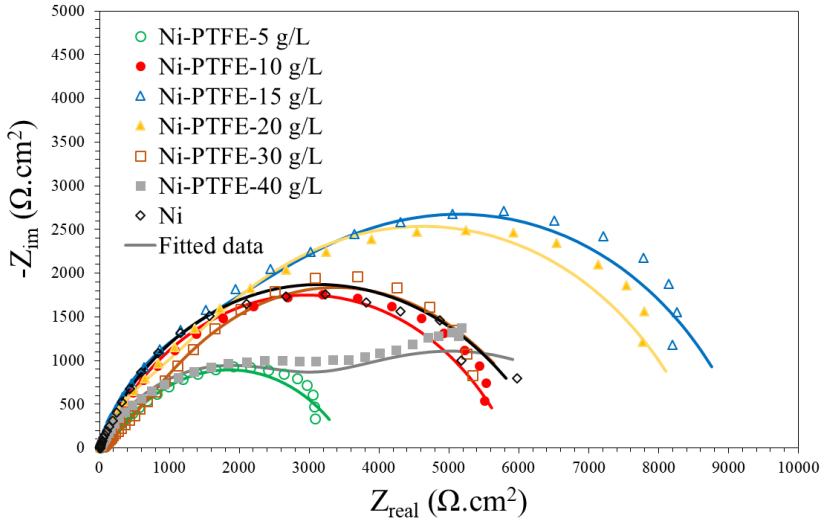
-Z_im (Ω.cm²)
Z_real (Ω.cm²)
Ni-PTFE-5 g/L
Ni-PTFE-10 g/L
Ni-PTFE-15 g/L
Ni-PTFE-20 g/L
Ni-PTFE-30 g/L
Ni-PTFE-40 g/L
Ni
Fitted data

b

Fig. 10

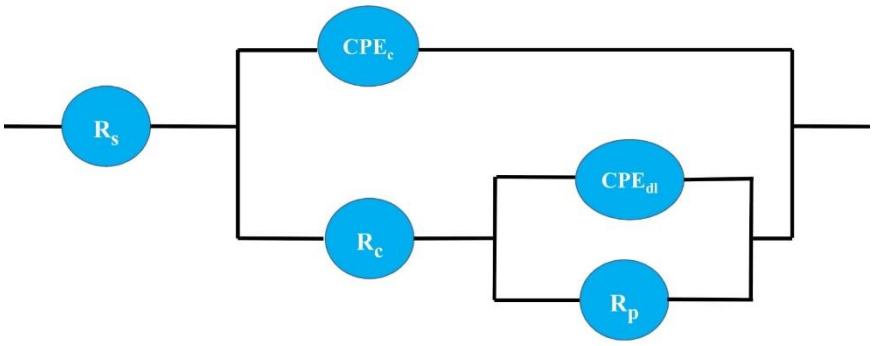

Fig. 11

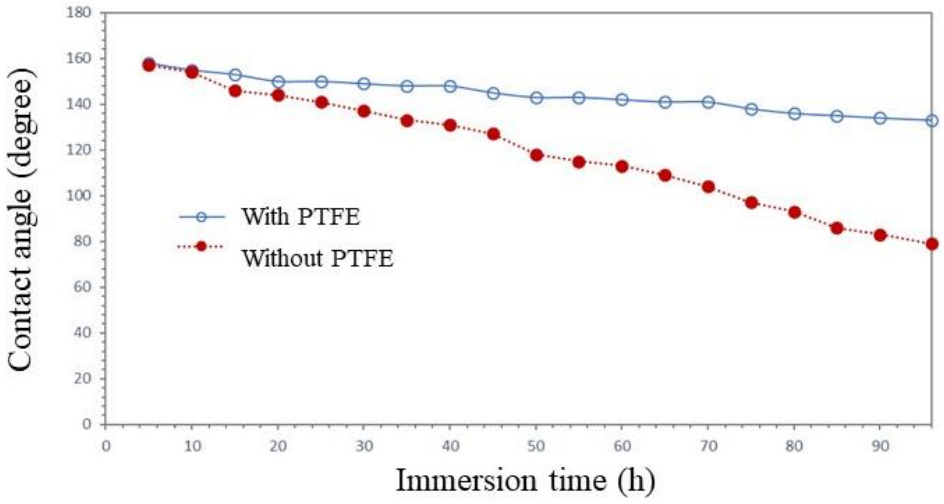
Contact angle (degree)
180
160
140
120
100
80
60
40
20
0
0
10
20
30
40
50
60
70
80
90
Immersion time (h)
With PTFE
Without PTFE

Fig. 12

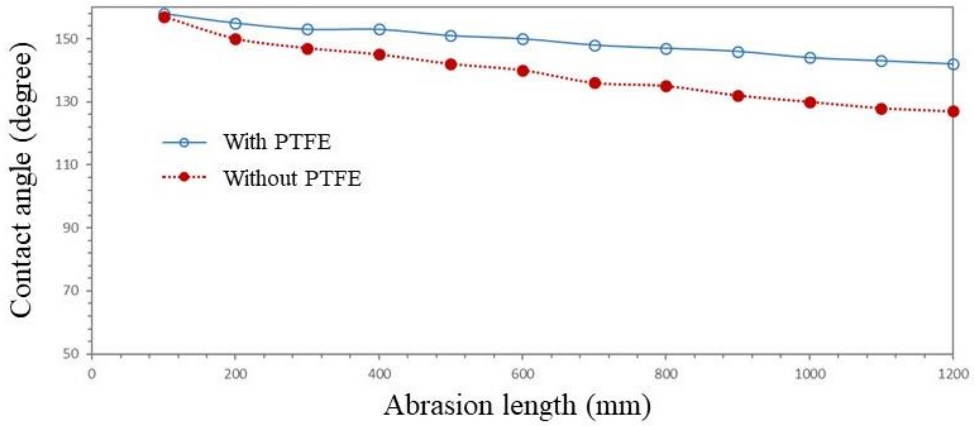
Contact angle (degree)
150
130
110
90
70
50
0
200
400
600
800
1000
1200
Abrasion length (mm)
With PTFE
Without PTFE

Fig. 13

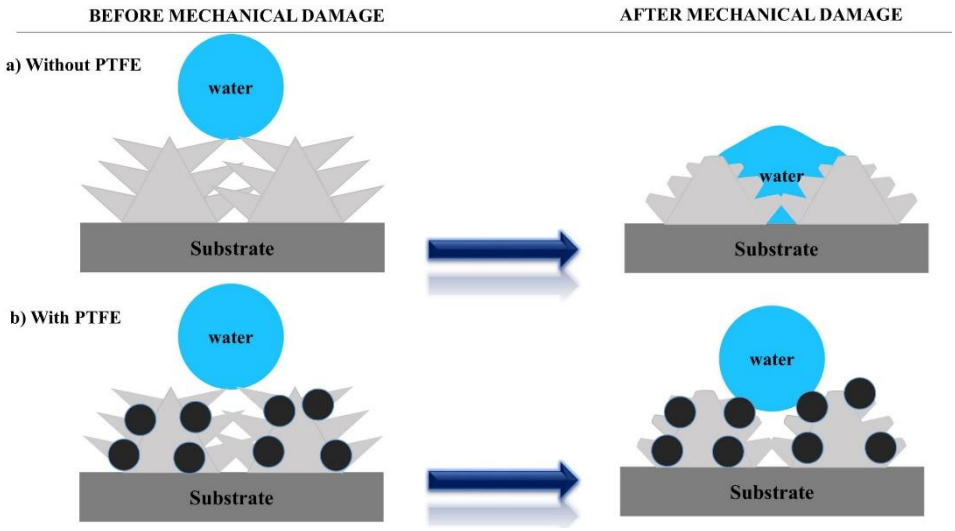
BEFORE MECHANICAL DAMAGE
AFTER MECHANICAL DAMAGE
a) Without PTFE
water
Substrate
water
Substrate
b) With PTFE
water
Substrate
water
Substrate

Fig. 14

Table 1.

Component	Amount (g/L)
$NiCl_2.6H_2O$	238
H_3BO_3	31
$C_2H_{10}Cl_2N_2$	200
CTAB	0.1
PTFE particles	5, 10, 15, 20, 30, 40

Table 2.

PTFE (g/L)	β_a (mV/decade)	β_c (mV/decade)	E_{corr} (mV.vs.SCE)	i_{corr} (µA/cm^2)
0	96.5	140	-29	2.28
5	31	69	-244	3.1
10	68	69	-335	2.2
15	73	67	-180	0.3
20	63	61	-189	0.54
30	70	68	-244	2.9
40	104	55	-261	3.6

Table 3.

PTFE (g/L)	R_s ($\Omega.cm^2$)	CPE_c ($\mu F/cm^2$)	n_c	Rc ($\Omega.cm^2$)	CPEdl ($\mu F/cm^2$)	n_{dl}	R_p ($\Omega.cm^2$)
0	11.3	21	0.62	322	185	0.92	6125
5	11.2	62	0.72	112	236	0.92	3123
10	12.3	36	0.71	412	126	0.86	5846
15	10.4	16	0.62	612	59	0.81	9236
20	10.6	23	0.67	592	67	0.79	8426
30	13.2	32	0.61	389	156	0.75	6124
40	12.3	53	0.52	126	192	0.71	5423

Rs: Solution resistance; R_c: Coating resistance; R_p: Polarization resistance.
CPE_c: Constant phase element of the coating;
CPE_{dl}: Constant phase element of the electrical double layer. (n is the CPE exponent)